CHAPTER 11

Cancer Therapy

S. Zanganeh[*,§], J.Q. Ho[†], R. Spitler[*], T. Jafari[‡], N. Khakpash[‡], M. Erfanzadeh[‡], M. Pauliah[§]

[*]Stanford University, Stanford, CA, United States
[†]Middlebury College, Middlebury, VT, United States
[‡]University of Connecticut, Storrs, CT, United States
[§]Sloan Kettering Institute for Cancer Research, New York, NY, United States

11.1 INTRODUCTION

Cancer is one of the biggest disease challenges and leading causes of death [1]. Imaging represents a key step in the clinical management of cancer [2–11]. Magnetic resonance imaging (MRI) is one of the biomedical imaging modalities with a wide range of applications in cancer diagnosis and therapy [8]. One advantage of MRI is its high-contrast capability of imaging organs and tissues [12]. Other imaging modalities, such as X-rays, have reduced contrast quality and may even result in negative outcomes, including misdiagnosis of medical conditions [13]. Despite many advantages, MRI has limited sensitivity. In order to improve sensitivity and image contrast, contrast agents (CAs) are often required to assess its pathophysiological state [14] even without surgical intervention. Innovations in nanomaterials have overcome the drawbacks of traditional CAs by increasing MRI image contrast [15]. The distinct physicochemical properties of nanomaterial-based CAs allow them to be injected and transported easily in the body to improve diagnostic imaging tests [16]. Nanoparticles exhibit superior physicochemical properties, and they are widely applied in biomedical imaging and cancer therapeutics [17,18]. Furthermore, nanomaterials can be functionalized in many ways and may serve both diagnostic and therapeutic purposes, such as utilizing their optical and magnetic properties to combine targeted drug delivery with medical imaging [16,19–21]. Additionally, using these multimodal systems for cancer treatment has led to favorable outcomes and numerous clinical studies [22]. Widder and Senyei [23] proposed using nanoparticles in imaging scans in 1978. A category of nanoparticles widely used in MRI is superparamagnetic iron oxide nanoparticles (SPIONs) [24]. SPIONs possess a number of advantages over typical CAs [25]. Their benefits include superior detection sensitivity, greater biocompatibility and

Iron Oxide Nanoparticles for Biomedical Applications
https://doi.org/10.1016/B978-0-08-101925-2.00010-3

reduced toxicity, and longer retention time [25,26]. In addition, SPIONs are considered safe for chronic kidney disease patients [13]. Their magnetic properties can also be altered based on their size, shape, and structure, and they can be localized to a specific target using conjugation with target-specific ligands [27]. Nanoparticles also enable medical professionals to obtain more detailed images of anatomy, which are crucial for delivering drugs and treating tumors [28]. In oncology, iron oxide nanoparticles were first implemented clinically to diagnose lymph node metastases [29]. Studies on lymph node metastasis detection have demonstrated that SPIONs provide greater diagnostic precision, sensitivity, and specificity than unenhanced MRI [29,30]. Additionally, inflammation from cardiac, carotid, and aortic disease can all be detected using ultrasmall SPIONs (USPIONs) [27]. Although its future implications in clinical practice have yet to be discovered, USPION-enhanced MRI is already pertinent to the diagnosis of many cardiovascular and other diseases [31].

Currently, research is concentrated on creating multifunctional theranostic nanomaterials for diagnostic and therapeutic purposes [22]. However, there are obstacles that need to be addressed.

Here, we provide an overview of the characteristics and application of iron oxide nanoparticles as a main component of cancer diagnosis and therapy.

11.2 THE ROLE OF MAGNETIC IRON OXIDE IN CANCER THERAPY

Magnetic iron oxide nanoparticles have been extensively used as CAs for targeted delivery of both large and small biological molecules to the cancer microenvironment. Primarily, many investigators are working to understand the theranostic characteristics of magnetic iron oxide nanoparticles during cancer treatment [8]. Various chemical techniques are used to synthesize high-quality magnetic nanoparticles, some of which include coprecipitation [32], thermal decomposition [33], sol-gel [34,35], and solvothermal reaction [36]. Once the magnetic core (e.g., Fe_2O_3 [34] Fe [37], and FePt [38]) is synthesized, a suitable coating is usually appended to the surface [39]. The coating prevents assemblage of the colloidal suspension and increases biocompatibility [39,40]. Some common coatings consist of natural and synthetic polymers, such as dextran and carboxymethylated dextran [24,41,42], alginate [43–45], starch [46], polyethylene glycol (PEG) [32,47], poly(D,L-lactide-co-glycolide) [48], and organosilane

[49,50]. Magnetic nanoparticles have also been coated by small charged molecules, such as amino and dimercaptosuccinic acids, as well as hydroxamate and citrate [51].

Of the various types of magnetic nanoparticles, SPIONs have been investigated for their promising biomedical applications [52,53]. SPIONs can be created using numerous methods, including standard iron precursor precipitation [54], thermal decomposition [55], hydrothermal synthesis [56], microemulsion, sol-gel synthesis [57], and the polyol method [54]. The process of SPION synthesis is complex [58]. Thermal decomposition is known to lead to high monodispersity in SPIONs [59]. Numerous studies have investigated the application of SPIONs as CAs for MRI [41,60]. Specifically, SPIONs have tunable properties like magnetism, size, and facile conjugation with biologically functional units that make them ideal platforms for modifiable CAs [61]. Currently, the most popular small-molecule CAs in clinical MRI practice are Gd-based. However, in certain patients, these Gd-based CAs have caused serious complications, such as nephrogenic systemic fibrosis [25]. Representing an alternative CA, SPIONs have unique magnetic properties that produce strong shortening effects and exhibit high biocompatibility [26]. Another advantage of SPIONs is that the amount of iron in a typical CA injection per person (0.5 mg/kg) is comparable with the 20–25 mg daily requirement per person, with humans having a large iron pool of 3–5 g [62]. Moreover, biodegraded iron can safely join the iron pool in the body and engage in physiological iron homeostasis [25]. Furthermore, renal clearance is not required because the reticuloendothelial system captures SPIONs, metabolizes them, and integrates the iron into the body's natural iron cycle [63].

The distinct properties of SPIONs allow them to have enormous versatility in biomedical applications spanning from cancer diagnostic applications in improving the contrast of MRI, magnetic particle imaging, and photoacoustic imaging [64] to drug delivery, cell labeling and tracking, and magnetic hyperthermia treatment [65]. In addition, SPIONs are used in tumor imaging and therapy (Fig. 11.1). Because of the enhanced permeability and retention effect, SPIONs administered systemically favor passive accumulation at tumor sites. SPIONs in the range of 10–100 nm are considered a suitable size for attaining an optimal enhanced permeability and retention effect with localization improvement [66]. Many active targeting strategies have been applied to aid SPION accumulation at tumor sites to enable high sensitivity and specificity [67]. For example, one popular method for producing glioma-targeted SPIONs involves the use of a

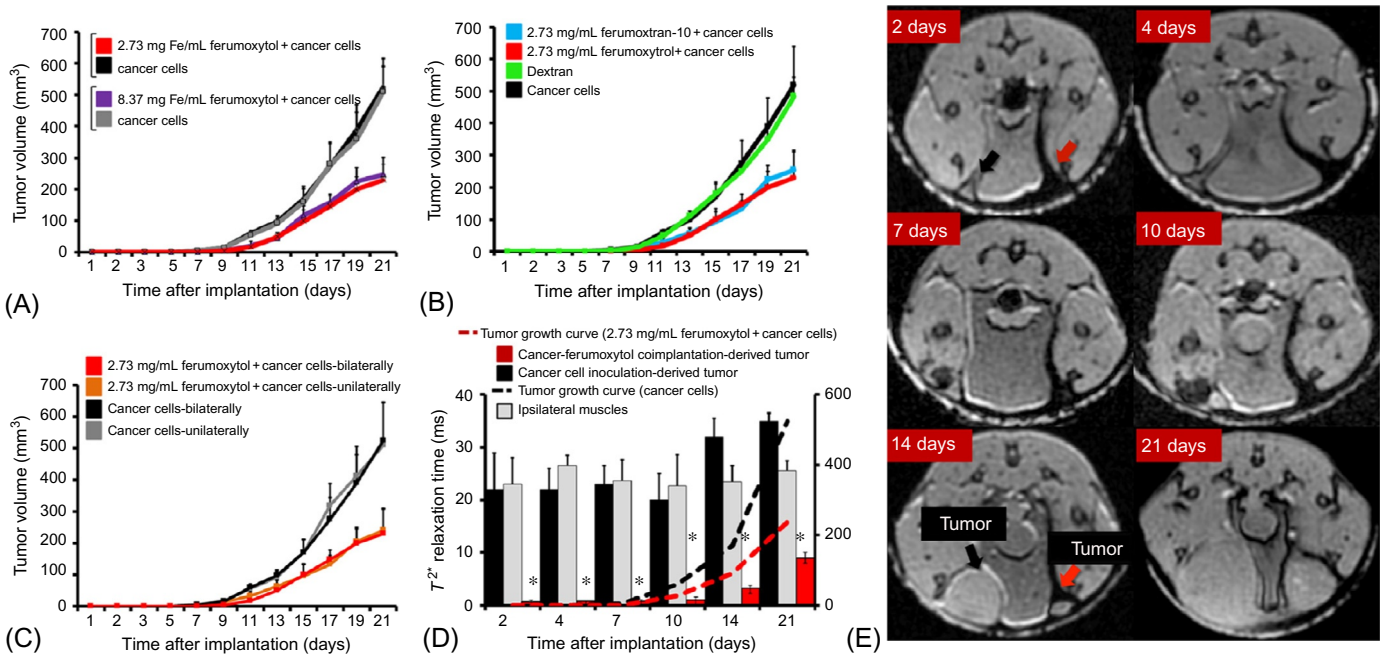

Fig. 11.1 Iron oxide nanoparticles (ferumoxytol) inhibit growth of breast tumors. Mice were implanted with the indicated number of cancer cells in the mammary fat pad, with and without ferumoxytol. (A) Ferumoxytol similarly inhibited tumor growth compared with untreated controls at two different local iron (Fe) concentrations of 2.73 mg Fe/ml. (B) Tumor growth was significantly inhibited compared with untreated controls by two different iron oxide nanoparticle compounds. (C) No significant difference in tumor sizes was observed between mice inoculated unilaterally and those inoculated bilaterally. (D) Corresponding serial quantitative MR signal of ferumoxytol coimplanted and untreated cancer inoculation sites. (E) Corresponding representative T_2*-weighted axial gradient-echo MR images. *Red arrows (gray arrows in print versions)* indicate ferumoxytol-induced negative *(dark)* T_2* signal effects at ferumoxytol-cancer cell coimplantation sites, and *black arrows* indicate lack of T_2* signal effects at cancer-implantation-only sites. Tumor growth is delayed at the ferumoxytol-cancer cell coimplantation site [8].

multitude of glioma-specific targeting moieties such as peptides, peptidomimetics, proteins, antibodies, aptamers, and small molecules [65].

11.3 DIAGNOSTIC IMAGING AND CANCER THERAPY

Over the past decade, various applications of magnetic nanoparticles have been explored in nanomedicine and cancer research (Fig. 11.2). Potential uses include drug delivery, thermal therapy, and MRI [69]. The possibility that some nanomaterials may play major roles in diagnosing and treating cancers have been demonstrated through discoveries in nanoparticle technology [3–5,8,9,70]. As a principal diagnostic imaging modality, MRI has high spatial resolution, powerful contrast for soft tissue, superb anatomic detail, and the absence of ionizing radiation [71]. Since X-ray-computed tomography and positron emission tomography have raised concerns about radiation exposure, MRI may play a critically important role in the clinical diagnosis of diseases, such as cancer and inflammation [72]. The low sensitivity of MRI is an impediment to accurately detect cancers in early stages or fine anatomical alterations. However, magnetic nanoparticles represent a means to improve MRI contrast and address the low sensitivity of MRI [73].

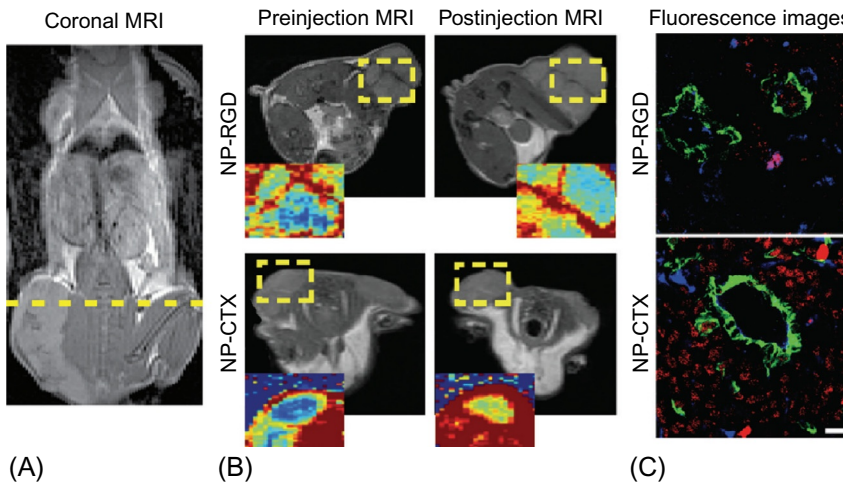

Fig. 11.2 Targeting iron oxide nanoparticles in the tumor microenvironment. (A) Coronal MR image of a mouse bearing tumors. (B) MR images of NP-CTX and NP-RGD treated mice. (C) Histological analysis of tumors showing the selective localization of NP-RGD with neovasculature and NP-CTX throughout the tumor. Color scheme for panel C—*green (light gray in print versions)*, anti-CD31 (mature endothelial cell marker); *blue (dark gray in print versions)*, anti-CD61 (neovasculature marker); and *red (medium gray in print versions)*, nanoparticles [68].

By resolving the drawbacks of a single imaging modality of MRI (low sensitivity, low spatial resolution, and small depth of penetration), many studies testing SPIONs with multiimaging modalities have recently described successful visualization enhancement [72]. Various imaging methods including MRI, positron emission tomography, single-photon emission computed tomography, and near-infrared fluorescence can be combined to generate synergistic data, which in turn permit cancer diagnosis at early stages and more definitive recognition of the molecular and metabolic properties of tumors [74]. However, SPIONs administered systemically have limited availability for multimodality imaging because they are susceptible to opsonization and reticuloendothelial system clearance [62]. Problems involving sensitivity and detection thresholds necessitate further research in these areas for the various imaging modalities. In addition, multifunctional iron oxide nanoparticles should be cautiously optimized during development because their properties are affected by the alteration of functional groups during conjugation [75]. Therefore, the possible interactions between components should be thoroughly investigated to guarantee complementarity in the complete design.

11.3.1 Characteristics of Iron Oxide Nanoparticle-Based Contrast Agents for Cancer Imaging and Therapy

Because of the unique physical and chemical properties, iron oxide nanoparticles should be further studied to uncover their potential applications in novel areas of bioengineering [17]. Compared with their bulk material counterparts, the relatively small size of nanoparticles results in greater surface area [42,76]. Other advantageous biomedical properties include biocompatibility and reactive surfaces [17]. These properties can help target biomolecules capable of conjugation to the nanoparticle surface, including antibodies, folates, and growth factors [77].

11.3.1.1 Size

Proper size is one of the key parameters for attaining high performance of SPIONs in cancer diagnosis and therapy. As the particle becomes smaller, its proportion of surface atoms relative to the entire particle increases, which causes the surface effect to become more prominent [78]. Because of incomplete coordination and diminished symmetry of the chemical environment around the surface magnetic cations, the magnetic structure on the surface is unlike the interior magnetic structure. Thus, the magnetic properties of iron oxide nanoparticles could be markedly influenced by the surface layer's

magnetic interaction [49]. Iron oxide nanoparticles that are substantially decreased in size to less than 50 nm cause individual particles to act as single magnetic domains and display negligible remanence and coercivity, which bring about their prevailing superparamagnetism and have a crucial effect on practical applications [38]. Furthermore, the ability of iron oxide nanoparticles to successfully overcome the biological defense system and vascular barriers in vivo is largely dependent on selecting the appropriate size. Depending on their diameter, iron oxide nanoparticles can be categorized as USPIONs (diameter < 50 nm), SPIONs (50 nm $>$ diameter > 1 μm), or micron-sized particles of iron oxide (diameter > 1 μm). For uniformly sized SPIONs, sizes of 4, 6, 9, and 12 nm express saturation magnetization values of 25, 43, 80, and 120 emu g^{-1} Fe, respectively [78].

Magnetic properties of the nanoparticle are notably impacted by large surface-to-volume ratios if its size is decreased to less than 3 nm. However, magnetic nanoparticles with diameters greater than 3 nm have extremely weak magnetic properties, because surface atoms exert little influence on magnetization. Moreover, iron oxide nanoparticles less than 2 nm in diameter demonstrate almost paramagnetic properties since most have canted spins. Recently, these minuscule IONs were examined for use as T_1 CAs [79]. Cellular uptake, biodistribution, and other pharmacokinetics are influenced by the size of the particle as well. In addition, nanoparticle transport into surrounding tissues is impacted by SPION size and pore spaces between the endothelial cells of blood vessels. Normally, following intravenous administration, the liver and spleen clear larger SPIONs ($>$1000 nm) faster than smaller particles, resulting in shorter blood circulation time. The kidneys usually filter out smaller SPIONs ($<$8 nm) [26]. Clinically approved SPIONs, which generally accumulate in the organs of the reticuloendothelial system such as the liver, spleen, and lymph node, typically come in medium sizes ranging from 10 to 300 nm [25]. Therefore, optimizing iron oxide nanoparticle size is crucial for preventing rapid removal by the body's immune system and allowing adequate accumulation in the target tissue or organ.

11.3.1.2 Shape

Aside from the size, the shape of iron oxide nanoparticles also has a significant effect on their properties. While the majority of SPIONs designed as MRI probes are spherical, other shapes (rhombic, ellipsoidal, cubic, crystal, flower, and cube) with useful magnetic properties have also been described [80,81]. Magnetic nanostructures are especially fascinating because of the connections

between their shape and function. The material morphology of nanostructures strongly affects their physical and chemical properties. Understanding this relationship can increase the likelihood of finding novel applications in many scientific and technological domains, such as magnetism and electronics [82]. The synthesis of spherical SPIONs has received enormous attention because, compared with other shapes, their synthesis can be managed by less complicated means. Consequently, the uniformity of spherical SPIONs can also be better controlled than with other shapes [26]. Control over the shape of nanostructures can be accomplished, in general, by tuning the growth rate in specific crystallographic directions. With regards to controlling the shapes of nanostructures, choosing the appropriate surfactant continues to be a major challenge. For instance, spherical, cubical, and star-like nanocrystals formed from oleic acid/oleylamine ratio adjustments have been systemically studied [81]. The oleic acid, with its carboxylic group, binds tightly to specific crystal facets of the original nuclei to create a stabilizing layer. While the amine group in oleylamine acts as an important reduction agent, in this case, it binds rather weakly onto the crystal surface. Concerning nanocube shape, a morphological progression follows a temporal succession that begins with spherical, then progresses to a spherical-to-cubic intermediate, to cubic, and finally to corner-grown shapes of nanocubes. Zhao and colleagues announced new findings in equivalent monodisperse magnetic nanostructures that have corner-grown morphology [80]. When they added chloride anions as a capping agent, they found a significant effect on the nanostructures, forming specific morphologies.

Besides zero-dimensional magnetic nanocrystals, one-dimensional nanostructures may be promising for multiple magnetic and biomedical purposes as well [83,84]. Mohapatra and colleagues altered the iron oxide morphology into a rod-like shape of 30–70 nm long and with a diameter of 4–12 nm to create an efficient MRI CA that had a large r_2 relaxivity value of 608 $mM^{-1}\ s^{-1}$. Larger surface area and anisotropic morphology improved the MRI contrast of nanorods. This larger surface area causes a greater perturbation of the magnetic field over a larger volume, leading to higher efficacy for outer sphere protons. The magnetic field induced by a rod is greater than that of spherical geometry. Thus, nanorods have higher r_2 relaxivity due to the stronger magnetic field over a large volume [85].

Recent studies have demonstrated that MRI magnetic properties and hence therapeutic utility could be theoretically and experimentally affected by three-dimensional magnetic nanostructures that are aggregation-based (clusters or assemblies) crystals [86,87]. After packaging SPION nanoclusters

into a controlled size using hyperbranched polyglycerol, Smith and colleagues [86] determined that the nanoclusters had a substantial relaxivity of 719 mM^{-1} s^{-1}, near their theoretical maximum. For identifying regions of defective vasculature in an ischemic murine hind limb, these nanoclusters could decrease the iron dosage for MRI 5- to 10-fold more than with traditional administrations during preclinical studies. Using a cationic-neutral double-hydrophilic poly (*N*-methyl-2-vinyl pyridinium) iodide-*block*-poly (ethylene oxide) diblock copolymer (P2QVP-*b*-PEO), Tahka et al. synthesized stable poly(ethylene oxide)-coated clusters from mediating the self-assembly of protein-cage-encapsulated iron oxide (γ-Fe_2O_3) nanoparticles (magnetoferritin). By managing nucleation/growth dynamics [87], Xie et al. created very organized, self-assembled three-dimensional nanoclusters that can have sharp or round edges [81]. They discovered that reducing nucleation duration can lead to inadequate nucleation and hasten the growth process of nanocrystals afterward, causing larger, star-like nanocrystals to develop. Further aligned for reciprocal assembly, the nanocrystals slowly form preliminary "branched" nanoclusters so that the magnetostatic energy from their size-dependent magnetic dipolar interactions will be minimized [81].

11.3.1.3 Composition

The magnetic properties of iron oxide nanoparticles are heavily influenced by the strategy in which iron oxide nanoparticles are doped with magnetically susceptible elements, so that other transition metal M^{2+} dopants replace Fe^{2+} ions [82]. Iron ion distribution in octahedral and tetrahedral sites of spinel structure impacts the magnetic property of magnetite (Fe_3O_4) nanoparticles [88]. Ferromagnetic coupling between magnetic spins of ions and antiferromagnetic coupling with tetrahedral sites occur in the octahedral sites. The magnetic spins in the octahedral and tetrahedral sites cancel out, because the numbers of Fe^{3+} ions on both sites are equal. Hence, the net magnetic moment is caused by the magnetic spins of only Fe^{2+} ions in the octahedral sites. One of the methods for controlling the magnetic properties of nanoparticles with spinel structures is to substitute Fe^{2+} ions with other divalent transition metal ions, including Mn^{2+}, Co^{2+}, Ni^{2+}, and Zn^{2+} ions. The net magnetic moments are proportional to the magnetic spins of divalent ions, excluding Zn^{2+}. Containing five unpaired d-orbital electrons, Mn^{2+} ions display the strongest magnetic moment among the divalent ions. Because r_2 relaxivity primarily depends on the saturation magnetization, $MnFe_2O_4$ nanoparticles have an r_2 relaxivity of 358 mM^{-1} s^{-1}, which is greater than the 218 mM^{-1} s^{-1} of Fe_3O_4 nanoparticles.

While the inorganic core of iron oxide nanoparticles dictates their physical properties, their surface properties serve important functions as well, particularly their effective interfacing (e.g., ensuring biocompatibility and specific localization) with biological systems, like proteins, cells, and tissues [72]. Surface modification of iron oxide nanoparticles is crucial for making them more stable, biocompatible, and functional and has been broadly investigated for in vivo biomedical applications.

For the surface engineering of SPIONs, the three central design considerations are stability, biocompatibility, and blood circulation time. Selecting a suitable polymer coating is primarily determined by its designed application. The majority of the SPIONs that are currently clinically approved have cores made of inorganic iron oxide and are coated with hydrophilic polymers, including but not limited to polysaccharide (i.e., dextran and its derivatives) and poly(ethylene glycol). The hydrophilic polymer coatings are critical for modulating the circulation time and biodistribution of SPIONs within the body. SPIONs that are not surface coated are unstable colloidal elements in solutions and susceptible to agglomeration and even precipitation in aqueous and physiological surroundings. However, it has been demonstrated that surface engineering and assembly structures of SPIONs influence their r_1/r_2 relaxations [25].

Recent developments have led to many ligand-conjugation strategies that enable high colloidal stability in aqueous biofluids and prevent aggregation arising under physiological conditions for IONs [89]. Adsorption of coating material onto the particle surface is a frequently utilized technique for surface coating. Generally, for in vivo application, iron oxide nanoparticles can be modified by the biologically inert polymer chains of a conventional ligand. Modifying the surface of iron oxide nanoparticles with PEG (PEGylation) may enhance stealth properties [90]. Aside from coating iron oxide nanoparticles with PEG, other block copolymers, including polyaniline [91] and polystyrene [92], can be utilized. USPIONs have been coated with polypyrrole, a conjugate polymer with absorption in near-infrared range, to acquire a multifunctional ION@PPy nanocomposite. Using a layer-by-layer method, the nanocomposite is then additionally modified by the biocompatible PEG to achieve high stability in physiological solutions [93].

Utilizing cross-linkable small molecules as bifunctional ligands greatly improves the structural stability of iron oxide nanoparticles, while their hydrodynamic diameters only increase slightly. For iron oxide nanoparticle surface modification, other ligands, such as the polysaccharides, acids, and

amines, are commonly applied as well [94]. Ozdemir et al. successfully introduced a new class of peptide-coated SPIONs to image tumors in vivo using MRI [95]. They reported a significant MRI signal enhancement of breast tumor tissue after the amphiphilic peptide-coated SPIONs (SPION/K-PA) were administered, demonstrating that the nanocomposite system has considerable potential as a negative MRI CA. However, the MRI signal's long-term consistency was revealed by in vivo observation of SPION/K-PA, and the absence of material accumulating in reticuloendothelial system organs was shown by histological analysis.

For noncovalent binding to the iron oxide nanoparticle surface, another method is based on hydrophobic effects as follows. Colloidal aggregates that are lipid-based, including liposomes, microemulsions, and micelles, can transport hydrophilic substances in the aqueous lumen and hydrophobic substances in the interior of the lipid membrane through this technique. According to one approach, the IONs and lipid undergo coprecipitation first, followed by redispersion in water [96].

To shield from oxidation or degradation of the cores, reactions in chemical conjugation, redox, and transmetalation, among other techniques, can be used to deposit certain precious metals (Au/Ag/Pt) and inorganic materials on magnetic nanoparticles. Aside from precious metal coatings, certain inorganic materials like silica [47] and carbon coatings have superior chemical and thermal stability, have surfaces that can be easily modified, and are biocompatible [17].

11.4 CONCLUSION

Recent developments in application of iron oxide nanoparticles in cancer therapy enable not only tumor destruction but also disruption of other essential components of the cancer microenvironment. Additionally, gains made in related areas of cancer imaging and cell tracking have enabled earlier detection using these changes as predictive imaging biomarkers. In this way, tumor growth can be monitored directly at the tumor site, while such changes as cellular infiltration, migration, and invasion along with structural changes in the surrounding tissues can improve clinical assessment. Furthermore, iron oxide-mediated direct immune activation can be utilized as a strategy for stimulating the immune system to specifically recognize and target cancer cells for elimination. Yet, there are still a number of challenges that will need to be addressed in order to limit toxicity and make these new approaches feasible for clinical translation. Some of the challenges still

to be addressed include off-target effects, nonspecific immune activation, and limited control over intracellular localization. However, the benefits of overcoming these challenges are significant such as improved control of biodistribution and transport kinetics, site-specific targeting, immunotherapeutic interventions, and likely others to come. For instance, the ability to effectively monitor and modulate the location and activation state of immune cells could lead to a better understanding of the complex cancer biology milieu and the development of more effective cancer therapies. With the constant emergence of novel approaches and applications of iron oxide nanoparticles, it is an exciting time for the field, which holds great potential for cancer therapy.

REFERENCES

[1] L.M. Coussens, Z. Werb, Inflammation and cancer, Nature 420 (2002) 860–867, https://doi.org/10.1038/nature01322.
[2] A. Abuteen, et al., The evaluation of NIR-absorbing porphyrin derivatives as contrast agents in photoacoustic imaging, Phys. Chem. Chem. Phys. 15 (2013) 18502–18509, https://doi.org/10.1039/c3cp52193a.
[3] U. Alqasemi, et al., Interlaced photoacoustic and ultrasound imaging system with real-time coregistration for ovarian tissue characterization, J. Biomed. Opt. 19 (2014) 76020, https://doi.org/10.1117/1.JBO.19.7.076020.
[4] N.C. Biswal, et al., Imaging tumor hypoxia by near-infrared fluorescence tomography, J. Biomed. Opt. 16 (2011) 066009, https://doi.org/10.1117/1.3589348.
[5] P.D. Kumavor, et al., Target detection and quantification using a hybrid hand-held diffuse optical tomography and photoacoustic tomography system, J. Biomed. Opt. 16 (2011) 046010, https://doi.org/10.1117/1.3563534.
[6] C. Xu, et al., Indocyanine green enhanced co-registered diffuse optical tomography and photoacoustic tomography, J. Biomed. Opt. 18 (2013) 126006, https://doi.org/10.1117/1.JBO.18.12.126006.
[7] Y. Xu, et al., Targeting tumor hypoxia with 2-nitroimidazole-indocyanine green dye conjugates, J. Biomed. Opt. 18 (2013) 66009, https://doi.org/10.1117/1.JBO.18.6.066009.
[8] S. Zanganeh, et al., Iron oxide nanoparticles inhibit tumour growth by inducing pro-inflammatory macrophage polarization in tumour tissues, Nat. Nanotechnol. 11 (2016) 986–994, https://doi.org/10.1038/nnano.2016.168.
[9] S. Zanganeh, et al., Photoacoustic imaging enhanced by indocyanine green-conjugated single-wall carbon nanotubes, J. Biomed. Opt. 18 (2013) 096006, https://doi.org/10.1117/1.JBO.18.9.096006.
[10] S. Zanganeh, et al., Enhanced fluorescence diffuse optical tomography with indocyanine green-encapsulating liposomes targeted to receptors for vascular endothelial growth factor in tumor vasculature, J. Biomed. Opt. 18 (2013) 126014, https://doi.org/10.1117/1.JBO.18.12.126014.
[11] F. Zhou, et al., Targeting tumor hypoxia: a third generation 2-nitroimidazole-indocyanine dye-conjugate with improved fluorescent yield, Org. Biomol. Chem. 13 (2015) 11220–11227, https://doi.org/10.1039/c5ob01460c.

[12] L.M. De Leõn-Rodríguez, A.F. Martins, M.C. Pinho, N.M. Rofsky, A.D. Sherry, Basic MR relaxation mechanisms and contrast agent design, J. Magn. Reson. Imaging 42 (2015) 545–565, https://doi.org/10.1002/jmri.24787.
[13] J. Tang, Y. Sheng, H. Hu, Y. Shen, Macromolecular MRI contrast agents: structures, properties and applications, Prog. Polym. Sci. 38 (2013) 462–502, https://doi.org/10.1016/j.progpolymsci.2012.07.001.
[14] A. Abdukayum, et al., Gadolinium complexes functionalized persistent luminescent nanoparticles as a multimodal probe for near-infrared luminescence and magnetic resonance imaging in vivo, Anal. Chem. 86 (2014) 4096–4101, https://doi.org/10.1021/ac500644x.
[15] J. Gallo, et al., CXCR4-targeted and MMP-responsive iron oxide nanoparticles for enhanced magnetic resonance imaging, Angew. Chem. Int. Ed. 53 (2014) 9550–9554, https://doi.org/10.1002/anie.201405442.
[16] M. Abdesselem, et al., Multifunctional rare-earth vanadate nanoparticles : luminescent labels, ACS Nano 8 (2014) 11126–11137.
[17] B.P. Burke, et al., Final step gallium-68 radiolabelling of silica-coated iron oxide nanorods as potential PET/MR multimodal imaging agents, Faraday Discuss. 175 (2014) 59–71, https://doi.org/10.1039/c4fd00137k.
[18] M.C. Daniel, D. Astruc, Gold nanoparticles: assembly, supramolecular chemistry, quantum-size-related properties, and applications toward biology, catalysis, and nanotechnology, Chem. Rev. 104 (2004) 293–346, https://doi.org/10.1021/cr030698+.
[19] M.S. Bradbury, M. Pauliah, P. Zanzonico, U. Wiesner, S. Patel, Intraoperative mapping of sentinel lymph node metastases using a clinically translated ultrasmall silica nanoparticle, Wiley Interdiscip. Rev. Nanomed. Nanobiotechnol. 8 (2016) 535–553, https://doi.org/10.1002/wnan.1380.
[20] M.S. Bradbury, et al., Clinically-translated silica nanoparticles as dual-modality cancer-targeted probes for image-guided surgery and interventions, Integr. Biol. 5 (2013) 74–86, https://doi.org/10.1039/c2ib20174g.
[21] A. Burns, H. Ow, U. Wiesner, Fluorescent core-shell silica nanoparticles: towards "Lab on a Particle" architectures for nanobiotechnology, Chem. Soc. Rev. 35 (2006) 1028–1042, https://doi.org/10.1039/b600562b.
[22] Z. Cheng, A. Al Zaki, J.Z. Hui, V.R. Muzykantov, A. Tsourkas, Multifunctional nanoparticles: cost versus benefit of adding targeting and imaging capabilities, Science (New York, N.Y.) 338 (2012) 903–910, https://doi.org/10.1126/science.1226338.
[23] A. Senyei, K. Widder, G. Czerlinski, Magnetic guidance of drug-carrying microspheres, J. Appl. Phys. 49 (1978) 3578–3583.
[24] D.G. You, et al., Dextran sulfate-coated superparamagnetic iron oxide nanoparticles as a contrast agent for atherosclerosis imaging, Carbohydr. Polym. 101 (2014) 1225–1233, https://doi.org/10.1016/j.carbpol.2013.10.068.
[25] R. Jin, B. Lin, D. Li, H. Ai, Superparamagnetic iron oxide nanoparticles for MR imaging and therapy: design considerations and clinical applications, Curr. Opin. Pharmacol. 18 (2014) 18–27, https://doi.org/10.1016/j.coph.2014.08.002.
[26] T. Lam, P. Pouliot, P.K. Avti, F.d.r. Lesage, A.K. Kakkar, Superparamagnetic iron oxide based nanoprobes for imaging and theranostics, Adv. Colloid Interface Sci. 199–200 (2013) 95–113, https://doi.org/10.1016/j.cis.2013.06.007.
[27] A.G. Ploussi, M. Gazouli, G. Stathis, N.L. Kelekis, E.P. Efstathopoulos, Iron oxide nanoparticles as contrast agents in molecular magnetic resonance imaging: do they open new perspectives in cardiovascular imaging? Cardiol. Rev. 23 (2015) 229–235, https://doi.org/10.1097/crd.0000000000000055.
[28] C. Felton, et al., Magnetic nanoparticles as contrast agents in biomedical imaging: recent advances in iron- and manganese-based magnetic nanoparticles, Drug Metab. Rev. 46 (2014) 142–154, https://doi.org/10.3109/03602532.2013.876429.

[29] L. Johnson, S.E. Pinder, M. Douek, Deposition of superparamagnetic iron-oxide nanoparticles in axillary sentinel lymph nodes following subcutaneous injection, Histopathology 62 (2013) 481–486, https://doi.org/10.1111/his.12019.
[30] M. Maddox, et al., Nanotechnology applications in urology: a review, BJU Int. 114 (2014) 653–660, https://doi.org/10.1111/bju.12782.
[31] C.G. Stirrat, et al., Ultra-small superparamagnetic particles of iron oxide in magnetic resonance imaging of cardiovascular disease, J. Vasc. Diagn. Interv. 2 (2014) 99–112, https://doi.org/10.2147/JVD.S50036.
[32] M. Anbarasu, M. Anandan, E. Chinnasamy, V. Gopinath, K. Balamurugan, Synthesis and characterization of polyethylene glycol (PEG) coated Fe_3O_4 nanoparticles by chemical co-precipitation method for biomedical applications, Spectrochim. Acta A Mol. Biomol. Spectrosc. 135 (2015) 536–539, https://doi.org/10.1016/j.saa.2014.07.059.
[33] Y. Eom, M. Abbas, H. Noh, C. Kim, Morphology-controlled synthesis of highly crystalline Fe_3O_4 and $CoFe_2O_4$ nanoparticles using a facile thermal decomposition method, RSC Adv. 6 (2016) 15861–15867, https://doi.org/10.1039/C5RA27649G.
[34] T. Jiang, et al., Synthesis of mesoporous γ-Fe_2O_3 supported palladium nanoparticles and investigation of their roles as magnetically recyclable catalysts for nitrobenzene hydrogenation, Appl. Catal. A Gen. 502 (2015) 105–113, https://doi.org/10.1016/j.apcata.2015.05.013.
[35] G.J. Owens, et al., Sol-gel based materials for biomedical applications, Prog. Mater. Sci. 77 (2016) 1–79, https://doi.org/10.1016/j.pmatsci.2015.12.001.
[36] F. Ooi, et al., A facile solvothermal synthesis of octahedral Fe_3O_4 nanoparticles, Small (2015) 1–5, https://doi.org/10.1002/smll.201401954.
[37] C. Langlois, et al., Fully crystalline faceted Fe–Au core–shell nanoparticles, Nano Lett. (2015), https://doi.org/10.1021/acs.nanolett.5b02273.
[38] K.L. Pisane, S. Singh, M.S. Seehra, Synthesis, structural characterization and magnetic properties of Fe/Pt core-shell nanoparticles, J. Appl. Phys. 117 (2015), https://doi.org/10.1063/1.4908304.
[39] T.D. Nguyen, K.-S. Kim, Functionalization of magnetic nanoparticles for biomedical applications, Korean J. Chem. Eng. 31 (2014) 1289–1305, https://doi.org/10.1007/s11814-014-0156-6.
[40] L. Momtazi, et al., Synthesis, characterization, and cellular uptake of magnetic nanocarriers for cancer drug delivery, J. Colloid Interface Sci. 433 (2014) 76–85, https://doi.org/10.1016/j.jcis.2014.07.013.
[41] M. Barrow, et al., Tailoring the surface charge of dextran-based polymer coated SPIONs for modulated stem cell uptake and MRI contrast, Biomater. Sci. (2015) 608–616, https://doi.org/10.1039/c5bm00011d.
[42] R. Borny, et al., Nucleophilic cross-linked, dextran coated iron oxide nanoparticles as basis for molecular imaging: synthesis, characterization, visualization and comparison with previous product, Contrast Media Mol. Imaging 10 (2015) 18–27, https://doi.org/10.1002/cmmi.1595.
[43] A. Bar-Shir, et al., Alginate-coated magnetic nanoparticles for noninvasive MRI of extracellular calcium, NMR Biomed. 27 (2014) 774–783, https://doi.org/10.1002/nbm.3117.
[44] J. Castello, M. Gallardo, M.A. Busquets, J. Estelrich, Chitosan (or alginate)-coated iron oxide nanoparticles: a comparative study, Colloids Surf. A Physicochem. Eng. Asp. 468 (2015) 151–158, https://doi.org/10.1016/j.colsurfa.2014.12.031.
[45] A. Teleki, F.L. Haufe, A.M. Hirt, S.E. Pratsinis, G.A. Sotiriou, Highly scalable production of uniformly-coated superparamagnetic nanoparticles for triggered drug release from alginate hydrogels, RSC Adv. 6 (2016) 21503–21510, https://doi.org/10.1039/C6RA03115C.

[46] C. Saikia, A. Hussain, A. Ramteke, H.K. Sharma, T.K. Maji, Crosslinked thiolated starch coated Fe_3O_4 magnetic nanoparticles: effect of montmorillonite and crosslinking density on drug delivery properties, Starch/Staerke 66 (2014) 760–771, https://doi.org/10.1002/star.201300277.
[47] B.P. Burke, et al., Chelator free gallium-68 radiolabelling of silica coated iron oxide nanorods via surface interactions, Nanoscale 7 (2015) 14889–14896, https://doi.org/10.1039/c5nr02753e.
[48] S. Minardi, et al., PLGA-mesoporous silicon microspheres for the in vivo controlled temporospatial delivery of proteins, ACS Appl. Mater. Interfaces 7 (30) (2015) 16364–16373, https://doi.org/10.1021/acsami.5b03464.
[49] T.S. Anirudhan, P.L. Divya, J. Nima, Synthesis and characterization of silane coated magnetic nanoparticles/glycidylmethacrylate-grafted-maleated cyclodextrin composite hydrogel as a drug carrier for the controlled delivery of 5-fluorouracil, Mater. Sci. Eng. C Mater. Biol. Appl. 55 (2015) 471–481, https://doi.org/10.1016/j.msec.2015.05.068.
[50] L.K. Mireles, E. Sacher, L.H. Yahia, S. Laurent, D. Stanicki, A comparative physicochemical, morphological and magnetic study of silane-functionalized superparamagnetic iron oxide nanoparticles prepared by alkaline coprecipitation, Int. J. Biochem. Cell Biol. (2015), https://doi.org/10.1016/j.biocel.2015.12.002.
[51] S. Sharifi, et al., Superparamagnetic iron oxide nanoparticles for in vivo molecular and cellular imaging, Contrast Media Mol. Imaging 10 (2015) 329–355, https://doi.org/10.1002/cmmi.1638.
[52] D. Edge, et al., Pharmacokinetics and bio-distribution of novel super paramagnetic iron oxide nanoparticles (SPIONs) in the anaesthetized pig, Clin. Exp. Pharmacol. Physiol. 43 (2016) 319–326, https://doi.org/10.1111/1440-1681.12533.
[53] I. Karimzadeh, et al., A novel method for preparation of bare and poly(vinylpyrrolidone) coated superparamagnetic iron oxide nanoparticles for biomedical applications, Mater. Lett. 179 (2016) 5–8, https://doi.org/10.1016/j.matlet.2016.05.048.
[54] R. Hachani, et al., Polyol synthesis, functionalisation, and biocompatibility studies of superparamagnetic iron oxide nanoparticles as potential MRI contrast agents, Nanoscale (2016) 3278–3287, https://doi.org/10.1039/C5NR03867G.
[55] L. Gonzalez-Moragas, S.-M. Yu, N. Murillo-Cremaes, A. Laromaine, A. Roig, Scale-up synthesis of iron oxide nanoparticles by microwave-assisted thermal decomposition, Chem. Eng. J. 281 (2015) 87–95, https://doi.org/10.1016/j.cej.2015.06.066.
[56] J. Li, X. Shi, M. Shen, Hydrothermal synthesis and functionalization of iron oxide nanoparticles for MR imaging applications, Part. Part. Syst. Charact. 31 (2014) 1223–1237, https://doi.org/10.1002/ppsc.201400087.
[57] S. Riaz, R. Ashraf, A. Akbar, S. Naseem, Free growth of iron oxide nanostructures by sol-gel spin coating technique—structural and magnetic properties, IEEE Trans. Magn. 50 (2014) 2301805.
[58] T.K.O. Vuong, et al., Synthesis of high-magnetization and monodisperse Fe_3O_4 nanoparticles via thermal decomposition, Mater. Chem. Phys. 163 (2015) 537–544, https://doi.org/10.1016/j.matchemphys.2015.08.010.
[59] R. Hufschmid, et al., Synthesis of phase-pure and monodisperse iron oxide nanoparticles by thermal decomposition, Nanoscale 7 (2015) 11142–11154, https://doi.org/10.1039/c5nr01651g.
[60] M. Borges, et al., Dual T_1T_2 MRI contrast agent based on hybrid SPION@coordination polymer nanoparticles, RSC Adv. 5 (2015) 86779–86783, https://doi.org/10.1039/C5RA17661A.
[61] N. Lee, T. Hyeon, Designed synthesis of uniformly sized iron oxide nanoparticles for efficient magnetic resonance imaging contrast agents, Chem. Soc. Rev. 41 (2012) 2575–2589, https://doi.org/10.1039/C1CS15248C.

[62] H. Ittrich, K. Peldschus, N. Raabe, M. Kaul, G. Adam, Superparamagnetic iron oxide nanoparticles in biomedicine: applications and developments in diagnostics and therapy, RoFo 185 (2013) 1149–1166, https://doi.org/10.1055/s-0033-1335438.
[63] M. Iv, et al., Clinical applications of iron oxide nanoparticles for magnetic resonance imaging of brain tumors, Nanomedicine 10 (2015) 993–1018.
[64] A. Tomitaka, H. Arami, S. Gandhi, K.M. Krishnan, Lactoferrin conjugated iron oxide nanoparticles for targeting brain glioma cells in magnetic particle imaging, Nanoscale 7 (2015) 16890–16898, https://doi.org/10.1039/c5nr02831k.
[65] H. Liu, et al., Imaging and therapy: from bench to bedside, Nanoscale 8 (2016) 7808–7826, https://doi.org/10.1039/c6nr00147e.
[66] J.D. Meyers, T. Doane, C. Burda, J.P. Basilion, Nanoparticles for imaging and treating brain cancer, Nanomedicine 8 (2013) 123–143.
[67] Y. Cheng, R.A. Morshed, B. Auffinger, A.L. Tobias, M.S. Lesniak, Multifunctional nanoparticles for brain tumor imaging and therapy, Adv. Drug Deliv. Rev. 66 (2014) 42–57, https://doi.org/10.1016/j.addr.2013.09.006.
[68] F.M. Kievit, M. Zhang, Surface engineering of iron oxide nanoparticles for targeted cancer therapy, Acc. Chem. Res. 44 (2011) 853–862, https://doi.org/10.1021/ar2000277.
[69] M. Branca, et al., Towards MRI T2 contrast agents of increased efficiency, J. Magn. Magn. Mater. 377 (2015) 348–353, https://doi.org/10.1016/j.jmmm.2014.10.086.
[70] A. Yadollahpour, Magnetic nanoparticles in medicine: a review of synthesis methods and important characteristics, Orient. J. Chem. 31 (2015) 271–277.
[71] T. Hussain, Q.T. Nguyen, Molecular imaging for cancer diagnosis and surgery, Adv. Drug Deliv. Rev. 66 (2014) 90–100, https://doi.org/10.1016/j.addr.2013.09.007.
[72] N. Lee, et al., Iron oxide based nanoparticles for multimodal imaging and magnetoresponsive therapy, Chem. Rev. 115 (2015) 10637–10689, https://doi.org/10.1021/acs.chemrev.5b00112.
[73] T.-H. Shin, Y. Choi, S. Kim, J. Cheon, Recent advances in magnetic nanoparticle-based multi-modal imaging, Chem. Soc. Rev. 44 (2015) 4501–4516, https://doi.org/10.1039/C4CS00345D.
[74] N. Xiao, et al., T1-T2 dual-modal MRI of brain gliomas using PEGylated Gd-doped iron oxide nanoparticles, J. Colloid Interface Sci. 417 (2014) 159–165, https://doi.org/10.1016/j.jcis.2013.11.020.
[75] W. Li, et al., Facile preparation of multifunctional superparamagnetic PHBV microspheres containing SPIONs for biomedical applications, Nat. Publ. Group (2016) 1–12, https://doi.org/10.1038/srep23140.
[76] Y. Xu, et al., Multifunctional magnetic nanoparticles for synergistic enhancement of cancer treatment by combinatorial radio frequency thermolysis and drug delivery, Adv. Healthc. Mater. 1 (2012) 493–501, https://doi.org/10.1002/adhm.201200079.
[77] A. Karmakar, et al., Raman spectroscopy as a detection and analysis tool for in vitro specific targeting of pancreatic cancer cells by EGF-conjugated, single-walled carbon nanotubes, J. Appl. Toxicol. 32 (2012) 365–375, https://doi.org/10.1002/jat.1742.
[78] D. Ling, N. Lee, T. Hyeon, Chemical synthesis and assembly of uniformly sized iron oxide nanoparticles for medical applications, Acc. Chem. Res. 48 (2015) 1276–1285, https://doi.org/10.1021/acs.accounts.5b00038.
[79] S.H. Lee, B.H. Kim, H.B. Na, T. Hyeon, Paramagnetic inorganic nanoparticles as T1 MRI contrast agents, Wiley Interdiscip. Rev. Nanomed. Nanobiotechnol. 6 (2014) 196–209.
[80] Z. Zhao, et al., Octapod iron oxide nanoparticles as high-performance T_2 contrast agents for magnetic resonance imaging, Nat. Commun. 4 (2013) 2266, https://doi.org/10.1038/ncomms3266.

[81] J. Xie, C. Yan, Y. Zhang, N. Gu, Shape evolution of "multibranched" Mn-Zn ferrite nanostructures with high performance: a transformation of nanocrystals into nanoclusters, Chem. Mater. 25 (2013) 3702–3709, https://doi.org/10.1021/cm402036d.
[82] J. Xie, N. Gu, Y. Zhang, Advances in nanotheranostics, in: Springer Series in Biomaterials Science and Engineering, vol. II, Springer Singapore, Singapore, 2016, pp. 39–73.
[83] F.N. Sayed, V. Polshettiwar, Facile and sustainable synthesis of shaped iron oxide nanoparticles: effect of iron precursor salts on the shapes of iron oxides, Sci. Rep. 5 (2015) 9733, https://doi.org/10.1038/srep09733.
[84] Z. Chen, et al., Controllable synthesis of amine-functionalized Fe_3O_4 polyhedra for lipase immobilization, CrstEngComm 18 (2016) 3124–3129, https://doi.org/10.1039/C6CE00269B.
[85] J. Mohapatra, A. Mitra, H. Tyagi, D. Bahadur, M. Aslam, Iron oxide nanorods as high-performance magnetic resonance imaging contrast agents, Nanoscale 7 (2015) 9174–9184, https://doi.org/10.1039/c5nr00055f.
[86] C.E. Smith, et al., Hydrophilic packaging of iron oxide nanoclusters for highly sensitive imaging, Biomaterials 69 (2015) 184–190, https://doi.org/10.1016/j.biomaterials.2015.07.056.
[87] S. Tahka, A. Laiho, M.A. Kostiainen, Diblock-copolymer-mediated self-assembly of protein-stabilized iron oxide nanoparticle clusters for magnetic resonance imaging, Chemistry (Weinheim an der Bergstrasse, Germany) 20 (2014) 2718–2722, https://doi.org/10.1002/chem.201304070.
[88] H. Cai, et al., Iron oxide nanoparticles: facile synthesis of Gd (OH) 3-doped Fe_3O_4 nanoparticles for dual-mode T1-and T2-weighted magnetic resonance imaging applications, Part. Part. Syst. Charact. 32 (2015) 918.
[89] Z. Zhang, et al., Facile synthesis of folic acid-modified iron oxide nanoparticles for targeted MR imaging in pulmonary tumor xenografts, Mol. Imaging Biol. (2015), https://doi.org/10.1007/s11307-015-0918-5.
[90] M.F. Attia, et al., One-step synthesis of iron oxide polypyrrole nanoparticles encapsulating ketoprofen as model of hydrophobic drug, Int. J. Pharm. 508 (2016) 61–70, https://doi.org/10.1016/j.ijpharm.2016.04.073.
[91] X. Tian, et al., Flower-like Fe_2O_3/polyaniline core/shell nanocomposite and its electroheological properties, Colloids Surf. A Physicochem. Eng. Asp. 498 (2016) 185–193, https://doi.org/10.1016/j.colsurfa.2016.03.054.
[92] Y. Xie, R. Sougrat, S.P. Nunes, Synthesis and characterization of polystyrene coated iron oxide nanoparticles and asymmetric assemblies by phase inversion, J. Appl. Polym. Sci. 132 (2015) 1–11, https://doi.org/10.1002/app.41368.
[93] X. Song, et al., Ultra-small iron oxide doped polypyrrole nanoparticles for in vivo multimodal imaging guided photothermal therapy, Adv. Funct. Mater. 24 (2014) 1194–1201, https://doi.org/10.1002/adfm.201302463.
[94] P. Yu, et al., Folic acid-conjugated iron oxide porous nanorods loaded with doxorubicin for targeted drug delivery, Colloids Surf. B Biointerfaces 120 (2014) 142–151, https://doi.org/10.1016/j.colsurfb.2014.05.018.
[95] A. Ozdemir, M.S. Ekiz, A. Dilli, M.O. Guler, A.B. Tekinay, Amphiphilic peptide coated superparamagnetic iron oxide nanoparticles for in vivo MR tumor imaging, RSC Adv. 6 (2016) 45135–45146, https://doi.org/10.1039/C6RA07380H.
[96] S. Jiang, A.A. Eltoukhy, K.T. Love, R. Langer, D.G. Anderson, Lipidoid-coated iron oxide nanoparticles for efficient DNA and siRNA delivery, Nano Lett. 13 (2014) 1059–1064, https://doi.org/10.1021/nl304287a.Lipidoid-coated.